RSC Advances

ROYAL SOCIETY OF CHEMISTRY

www.rsc.org/advances

Journal Name

ARTICLE

Layer-by-layer reduced graphene oxide (rGO)/Gold nanosheets (AuNSs) hybrid films: significantly enhanced photothermal transition effect compared with rGO or AuNSs films

Received 00th January 20xx,
Accepted 00th January 20xx

DOI: 10.1039/x0xx00000x

www.rsc.org/

Kun Nie[a], Qi An[a], Shengyang Tao*[b], Zepeng Zhang[a], Xinglong Luan[a], Qian Zhang[a], Yihe Zhang*[a]*

Photothermal materials prepared from graphene and Au nanoparticles have received increasing attentions in various fields ranging from smart devices to advanced medical therapies. In this report, we studied the photothermal transition effects of LbL AuNS/rGO (AuNS: Au nanosheets) films under laser irradiation at 940 nm, and comparisons were made with the film of rGO or AuNSs where single type of photothermal effective species exist. The results indicate that the hybrid LbL AuNS/rGO films displayed enhanced photothermal effects compared with the rGO or AuNSs films. The photothermal performance of the hybrid AuNS/rGO films deteriorated over repeated use or long-term laser irradiation, but the ultimate performance after irradiation was still better than that of the rGO or AuNS films. The hybrid film was able to load model drug methylene blue (MB), and release MB 4 times faster with NIR irradiation than without, suggesting potential application in the combined chemical and thermal therapies. Thus, the hybrid film of AuNS-rGO is recommended when short-term or few-cycle photothermal applications are required. In comparison, rGO multilayered film better suits long-term or repeated photothermal applications where stable photothermal performance are required.

Introduction

Photothermal transition materials have received remarkably increasing research attentions in cancer therapies, drug delivery, smart devices, and functional films.[1-5] Gold nanoparticles and graphene are being especially intensively studied. Gold nanoparticles (AuNPs) present adjustable surface plasmon resonance (SPR) band and could be programmed to absorb light through the entire visible range as well as the near infrared (IR) range.[6] They also serve as signal-enhancing agents in Raman and fluorescence spectra, thus are extensively used as multifunctional (sensors, imaging and therapy agents) platform in biomedical devices.[7-8] Reduced graphene oxide (rGO), possessing the abilities of both photothermal transition and drug loading, have been engineered into various therapy agents with the aid of chemical surface modification strategies.[9-11] In order to combine the advantages of AuNPs and rGO, hybrid materials prepared from both items have received increasing attentions.[12,13] For example, graphene-wrapped AuNPs were developed as multimodel cell imaging agents, as well as combined chemo and thermal therapy agents, with enhanced stabilities.[14] GO-wrapped surface-enhanced Raman scattering (SERS) tags (gold nanoclusters) served as advanced labeling, photothermal therapy, and monitoring-assistant platforms.[15] More interestingly, when the SPR band of AuNPs were tuned to the wavelength of the laser beam, a coupling between the gold nanoparticles and GO which lead to enhanced photothermal effect was observed in hybrid AuNP-GO nanoparticular composites.[16,17]

Layered films of AuNP-rGO hybrid material, in addition to the hybrid particular composites, also find wide applications as sensors, sample plate as well as matrix in mass spectrometry, electrocatalytic films, and light heating layers in intelligent devices.[18-20] Because of the simplicity of the technique, the versatility in the choices of building blocks, and the controllability down to the nanoscopic scope, layer-by-layer technique is among the most widely used strategy to prepared hybrid AuNP-rGO films.[18-27] Layer-by-layer (LbL) assembled film of AuNP-rGO film find potential applications as versatile coatings of biomedical apparatus or nanoparticles with the abilities of sustained release of drugs and light-induced heating.[28] For these reasons, understandings of pros and cons of the hybrid LbL AuNP-rGO film is of paramount importance in the optimization of device performance. However, the systematic study in term of photothermal transition effect of LbL AuNP-rGO film is still lacking.

In this report, we prepared LbL AuNP-rGO films and studied their photothermal transition effects. Considering the photothermal materials are widely used in vivo, the maximum

[a]Beijing Key Laboratory of Materials Utilization of Nonmetallic Minerals and Solid Wastes, National Laboratory of Mineral Materials, School of Materials Science and Technology, China University of Geosciences, Beijing, 100083Address here.
[b]Department of Chemistry, Dalian University of Technology, Dalian, Liaoning, P. R. China.

† Electronic Supplementary Information (ESI) available: SEM, AFM images and UV-vis spectra of AuNS, and UV-vis spectra of rGO. This material is available free of charge via the Internet at http://pubs.rsc.org. See DOI: 10.1039/x0xx00000x

absorbance of our films was adjusted to around 940 nm, which locates in the transparent window (800 ~ 1100 nm) of bio tissues. This special maximum absorbance was enabled by carefully choosing the shape of AuNPs, which were nanosheets of the shape of trigons or hexagons. The hybrid LbL films of these gold nanosheets (AuNSs) and rGO displayed enhanced photothermal effects compared with the film of rGO or AuNSs where single type of photothermal effective species exist. However, the performance deteriorated over repeated use or long-term laser irradiation for the hybrid film, caused by the melting of the AuNSs induced by heating. The hybrid film was able to load and release of model drug methylene blue, suggesting potential application in the combined chemical and thermal therapies. With laser irradiation, the amount of the released drug significantly increased. Thus, the hybrid film of AuNS-rGO is recommended when short-term or few-cycle photothermal applications are required. In comparison, rGO multilayered film better suits long-term or repeated photothermal applications where stable photothermal performance are required.

Materials and characterizations

Materials. graphene oxide(GO) was purchased from Nanjing XFNANO Materials Tech Co.,Ltd(XFNANO). Poly(allylamine hydrochloride)(PAH,Mw=15000 g/mol), Poly(acrylic acid)(PAA)(Mw=240 000 g/mol), Poly(vinyl pyrrolidone)(PVP)(K30,Mw=40,000 g/mol) were obtained from Sigma-Aldrich. Hydrogen peroxide(30 wt%) was purchased from Sinopharm Chemical Reagent Co. Ltd,(Beijing,China). Gold chloride($HAuCl_3 \cdot HCl \cdot 4H_2O$,A.R.,Mw=411.85 g/mol),Sodium borohydride($NaBH_4$,Mw=37.95 g/mol),Sodium citrate($Na_3C_6H_5O_7 \cdot 2H_2O$,Mw=294.10 g/mol),and Sodium hydroxide (NaOH,Mw=40.00 g/mol) were purchased from Beijing Chemical Works(Beijing, China). Gold nanosheets were synthesized as reported, and presented absorbance at around 520 nm and 940 nm (Figure S3).[29-31] Only ultra-pure water and deionized water were used in this study.

Characterizations. UV-visible spectra were obtained using a Hitachi U-3900H spectrophotometer. Zeta-potential values were measured using Zetasizer NanoZS90. Attenuated total reflection Fourier transform infrared (ATR-FTIR) spectra were recorded on Excalibur 3100 in the range of 4000~600 cm^{-1} with 4 cm^{-1} resolution by measuring the absorbance of the films with the silicon as substrate. The surface morphology of the polyelectrolyte multilayers was characterized using atomic force microscopy (AFM; Dimension 3100, Veeco, USA), tapping mode, where the scan rate is 1 Hz, 512 lines. The force was optimized for each sample to obtaine the minimum noise, and the scan size is indicated by the scale in the images. Scanning electron microscopy (SEM; JSM-7600F,Japan). Infrared laser of 940 nm was generated from a laser produced by Beijing Laserwave Optoelectronics Tech. Co., Ltd. The type of the laser source is diode-pumped semiconductor laser. The non-contact temperature meter was purchased from Fluke Corporation, and the instrumental error for temperature measurement is 0.2 ℃.

Preparation of PAH-modified rGO

The reduced graphene oxide(rGO) was synthesized by reducing graphene oxide(GO) at the presence of PAH. In detail, GO(0.005 g) was dissolved by Ultrasonic Cleaner in 20 ml deionized water as the starting material, and was placed into 100 ml Erlenmeyer flasks and PAH(pH=9, 4 mg/ml,30 ml) as well as 20 µl Hydrazine Hydrate was added. The reduction reaction was conducted at 80 degree for 2 h. After reduction, the synthesized reduced graphene oxide was positively charged.

Fabrication of layer-by-layer self-assembled(LBL) films

Quartz substrates were first cleaned by immersing in pihrania solution (vH_2SO_4/vH_2O_2=3:1, caution, corrosive!) for one hour followed by thorough washing with deionized water. Then the $(rGO/AuNS)_n$ films were prepared by dipping the substrates into the rGO-PAH dispersion (0.25 mg/ml) for 20 min and AuNS dispersion for 20 min alternatively, with washing using deionized water for 10 min and drying with N_2 in between, until the intended number of layers were obtained. $(rGO/PAH)_n$ and $(PAH/AuNS)_n$ films were obtained in similar manners, with rGO-PAH dispersion or AuNS dispersion was replaced by PAH solution (pH=9) or PAA solution (pH= 6), respectively.

Photothermal conversion under near-infrared (NIR) light laser irradiation

The photothermal effects of the rGO-modified substrates were studied by measuring the surface temperature of 100 µL water heated by the substrate induced by a NIR laser of 940 nm. The water was carefully added to a container whose bottom was the modified substrate and walls were made of PDMS. A square hole of 7×7 mm was opened in a PDMS sheet using a cutter knife. Then the sheet was pressed against the modified substrate to create the container. Thus the surface area of the drop of water was fixed by the shape of the container. The NIR laser irradiated from above the water surface from a fixed distance of 5 cm. The power of the laser was set to 0.7 W. The temperature of the water surface was probed by a non-contact infrared temperature measurement instrument. The averages of three data points were used in plotting the heating effect of the multilayers verses irradiation time.

Adsorption and sustained release of methylene blue (MB)

For the sustained-release experiment, substrates covered with $(RGO/AuNS)_5$ films were immersed in Methylene blue solution (0.01 mg/ml) for 24 hours. Afterwards, these quartz plates were dried with Nitrogen. Subsequently, these quartz plates were immersed into phosphate buffered solution (PBS, pH=7.4) for sustained release. NIR irradiation was applied from a distance of 2.0 cm at a power of 0.7 W if required. The amount of released MB was monitored by a UV-VIS spectroscopy every five minutes.

Results and discussion

The synthesized AuNS were a mixture of polygons and spherical particles, as displayed in Figure S1. AuNS of triangles dominant in the mixture, and the edge lengths of the triangles were roughly 100 nm. The thicknesses of the nanosheets were within 10-30 nm, and a typical height profile of the nanosheet was displayed in Figure S2. The Au nanosheets were wrapped by PVP polymers, as indicated by the characteristic FTIR peak of PVP at 1680 cm^{-1} in Figure S3.[32] The surface potential of Au nanosheets was -0.5 mV. The prepared AuNS presented surface plasmon resonance at around 520 nm and 940 nm (Figure S4). NIR light at around 940 nm was effectively absorbed by the Au plate and this light-absorbance capability can then be used in photothermal transitions.[33-34] rGO prepared in our method presented surface modifications of PAH as indicated by ATR-IR spectra (Figure S5),[35-36] and a positive surface charge of +45 mV. The AFM image indicated the thickness of the rGO was 4.2 nm (Figure S6). Multilayered hybrid films of rGO and AuNSs were prepared using LbL technique. The driving forces for the assembly of the multilayers should be mainly hydrogen bonding, since PVP presents strong capability to form hydrogen bonds because of the strong proton-accepting properties of the carbonyl group in the molecule.[37] Electrostatic attraction should also assisting the assembly of the multilayers. The sequential deposition of the LbL multilayers was followed by UV-vis spectra (Figure 1a). The characteristic absorbance of both rGO and AuNSs were clearly observed in the UV-vis spectra. The intensities of the absorbance bands at around 270 nm (corresponding to rGO, Figure S7) and at around 520 and 940 nm (corresponding to AuNSs) all increased almost linearly with the growth of the number of bilayers. The absorbance band at around 900 nm red-shifted with the increase of the number of bilayers, and the maximum absorbance shifted to approximate 950 nm for the $(rGO/AuNS)_{10}$ film. The hybrid multilayers absorbed light strongly in the region of near infrared, between 850 and 1100 nm. This region is also the transparent window of bio tissues. Thus the strong absorbance of the film in this region makes it potentially useful in in vivo photothermal transition devices. The multilayered of $(PAH/AuNS)_n$ and $(PAA/PAH\text{-}rGO)_n$ were also constructed in similar manners for comparison. The assembly processes were monitored via UV-vis spectra, and the linear relationship between the absorbance and the number of bilayers were obtained in both cases, indicating even growth of each bilayer in both cases (Figure 1b-c). The cross-section of the $(rGO/AuNS)_5$ film was observed using SEM (Figure 1d), and the image demonstrated that the film surface was scattered by nanoparticles, with dimensions around tens of nanometers. The thickness of $(rGO/AuNS)_5$, $(RGO\text{-}PAH/PAA)_5$, $(Au/PAH)_5$ multilayers are 35.4 nm, 17.9 nm, and 26.4nm, respectively, measured by AFM (Figure S8).

Since the hybrid multilayered film absorbed near infrared light strongly, we then wondered whether the film could be used as photothermal transition materials. To this end, we fabricated films of (rGO/AuNS)n, (PAA/PAH-rGO)n and (PAH/AuNS)n. For each type of multilayered films, the photothermal transition effect increased with growing number of bilayers (Figure 2a-c).

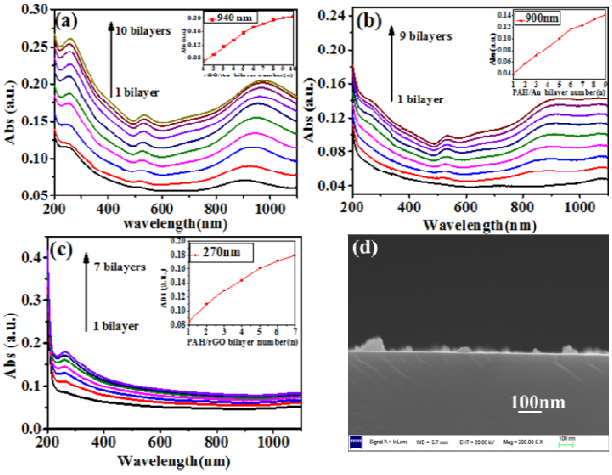

Figure 1. UV-vis spectra monitoring the layer-by-layer process of (a) $(rGO/AuNS)_{10}$ (b) $(PAH/AuNS)_9$, and (c) $(PAA/PAH\text{-}rGO)_7$ films, showing successful LbL assembly of each type of multilayers. (d) SEM image of cross-section of the $(rGO/AuNS)_{10}$ film.

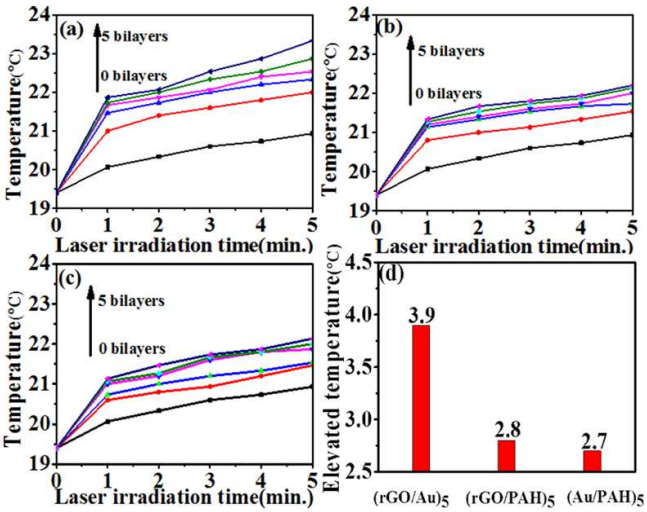

Figure 2. Photothermal effect indicated by elevated temperature of the (a) $(rGO/AuNS)_5$ (b) $(PAA/PAH\text{-}rGO)_5$, and (c) $(PAH/AuNS)_5$ films as a function of irradiation time. (d) Substrate temperature of the above mentioned film after an irradition period of 5 min.

After 5 min's irradiation, the temperature of the sample increased by 2.6, 2.9, 3.1, 3.5, and 3.9 degrees for the sample on the (rGO/AuNS)n film with n varied from 1-5. The temperature increased by 2.1, 2.3, 2.6, 2.7, and 2.8 degrees for the $(PAA/PAH\text{-}rGO)_n$ film, and by 2, 2.1, 2.5, 2.6, and 2.7 degrees for the $(PAH/AuNS)_n$ film, as n varied from 1 - 5. In comparison, the temperature of the sample on the blank quartz substrate increased by only 1.5 degrees. These results demonstrated that all three types of multilayers presented considerable photothermal effect. These results also demonstrated that given the total cycle of assembly identical,

the hybrid $(rGO/AuNS)_n$ film significantly outperformed the $(PAA/PAH\text{-}rGO)_n$ or $(PAH/AuNS)_n$ films. For example, the temperature raise was 3.9 degrees for the $(rGO/AuNS)_5$ film, but only 2.8 degrees and 2.7degrees for the $(PAA/PAH\text{-}rGO)_5$ or $(PAH/AuNS)_5$ films (Figure 2d).

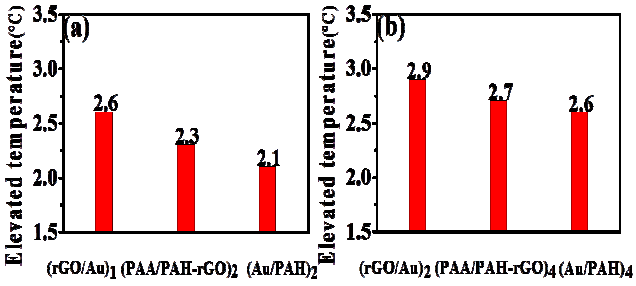

Figure 3. Substrate temperature after an irradiation period of 5 min for the (a) $(rGO/AuNS)_1$, $(PAH/AuNS)_2$ and $(PAA/PAH\text{-}rGO)_2$ and (b) $(rGO/AuNS)_2$, $(PAA/PAH\text{-}rGO)_4$ and $(PAH/AuNS)_4$ films.

Subsequently we wondered, whether the hybrid film presents higher transition effect compared with the $(PAA/PAH\text{-}rGO)_n$ or $(PAH/AuNS)_n$ films, where only one type of photothermal effective component exists. To this end, we fabricated films of $(rGO/AuNS)_1$, $(PAH/AuNS)_2$ and $(PAA/PAH\text{-}rGO)_2$. In these films, two layers (referred as two cycles of deposition in LbL assembly, although the accurate weight in each cycle for different species may differ) of photothermal effective species (rGO, or AuNS) were assembled. The hybrid film induced the largest temperature increase when the IR irradiation duration was longer than 2 min. After 5 min's irradiation, the temperature of the sample raised by 2.6 degrees for the hybrid film. $(PAA/PAH\text{-}rGO)_2$ film induced medium temperature increase of 2.3 degrees, and $(PAH/AuNS)_2$ film induced the minimum temperature increase of 2.1 degrees (Figure 3a). Further increase of the number of bilayers presented similar trend, verified by comparison of the photothermal effects of $(rGO/AuNS)_2$, $(PAA/PAH\text{-}rGO)_4$ and $(PAH/AuNS)_4$ films (Figure 3b). The $(rGO/AuNS)_2$ film induced the largest temperature increase of 2.9 degrees, the $(PAA/PAH\text{-}rGO)_4$ film medium of 2.7 degrees, and the $(PAH/AuNS)_4$ film the least of 2.6 degrees. These results indicated in the assembly process of LbL the combination of AuNS and rGO gave a synergistic effect. The hybrid film outperformed the films constructed using a single effective component, be it rGO or AuNS, provided that the number of layers of the effective components were identical.

However, further study revealed that the hybrid $(rGO/AuNS)_5$ film, effective in short-term photothermal transition experiments, suffered inconveniences in long-term or repeated applications. The absorbance of AuNS gradually diminished with the elongation of irradiation period, and after 60 min's irradiation, the absorbance at around 520 nm and 940 nm which were characteristic of the AuNSs disappeared completely (Figure 4a).

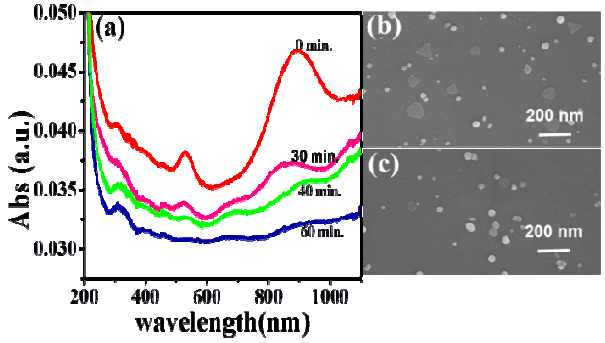

Figure 4. UV-vis spectra of $(rGO/AuNS)_5$ film after infrared irradiation period of 0, 30, 40, and 60 min. SEM images of the substrate surfaces (b) before and (c) after infrared irradiation of 60 min.

While the absorbance characteristic of rGO still existed. SEM images supported the deterioration of AuNS with irradiation. A typical SEM image of the multilayer surface is displayed in Figure 4b. AuNS and Au nanoparticles co-existed on the substrate surface before irradiation. In contrast, after cumulative irradiation for 50 min, AuNS largely disappeared on the surface and only quasi-spherical particles were observed.

Because of the deterioration of AuNS with irradiation, it's thus important to study the performance stability of the multilayers with repeated irradiation. The substrates of $(rGO/AuNS)_5$, $(PAA/PAH\text{-}rGO)_5$ and $(PAH/AuNS)_5$ films were then repeatedly irradiated and cooled down for over 10 cycles where the total irradiation time lasted over 50 min (5 min irradiation for each cycle, Figure 5). The hybrid film presented the highest temperature increase during each cycle and the temperature increase shrinked with repetition of cycles. About 15% of deterioration was observed after 10 cycles, but the temperature increase was still larger than that of the $(PAA/PAH\text{-}rGO)_5$ and $(PAH/AuNS)_5$ films. $(PAA/PAH\text{-}rGO)_5$ films presented stable heating performance of an increase of 2.7 degrees for each cycle.

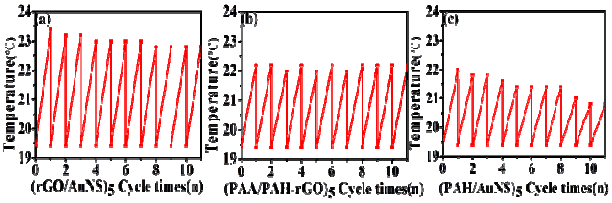

Figure 5. Substrate temperatures for cycles of 5 min's heatings with coolings in between for the (a) $(rGO/AuNS)_5$ (b) $(PAA/PAH\text{-}rGO)_5$, and (c) $(PAH/AuNS)_5$ films.

The heating performance of $(PAH/AuNS)_5$ films was poorest and deteriorate the most rapidly over repeated heating. About 54% of decrease of temperature rise was observed after 10 cycle heating. These results demonstrated that $(rGO/AuNS)_5$ films presented the most effective photothermal transition in relatively few repetition cycles, e.g., 10 cycles. However, the

deterioration of the photothermal effect should be considered, especially in long-term and repetitive uses.

In order to explore whether the hybrid $(rGO/AuNS)_5$ film (1.3*2.5 cm^2, both sides of the quartz substrate were covered by the film) effectively heat up a relatively large amount of water, we immersed the substrate into a vial that contained 10 ml water. After irradiation for 10 min, the temperature of the water increased from 19.4 degree to 22.2 degree. This result demonstrated that the film, although as thin as less than 100 nm, effectively warm up surrounding environment.

In the last step, we explored the loading and release capacities of the hybrid film $(rGO/AuNS)_5$.(Figure 6 & S9) The film was able to load MB by passive infiltration. Immersed in PBS, the loaded MB diffused out into solution gradually. It's worth noticing that irradiation remarkably increased the released amount of MB. With irradiation, a large proportion of MB (78% of the maximum released amount) was released quickly in the first 20 min. Then the release continued in a slower manner. Till around 70 min, the released amount of MB reached a plateau and no longer increased. In the meantime, the temperature of the solutions (3 mL) increased by only approximate 2 degrees with irradiation. In clear comparison, the substrate without irradiation released much less MB, whose amount was only 22% the amount released under irradiation. This clear comparison between the release capability with and without irradiation demonstrated that the hybrid multilayer only release the small molecules in effective manners under irradiation. Thus the film would have potential applications as molecule reservoirs. The small molecules were largely kept in the film and were only able to be effectively released under IR trigger at intended occasions. The release profile of the hybrid film demonstrated that controlled release could be obtained with the hybrid $(rGO/AuNS)_5$ film. The high controllability

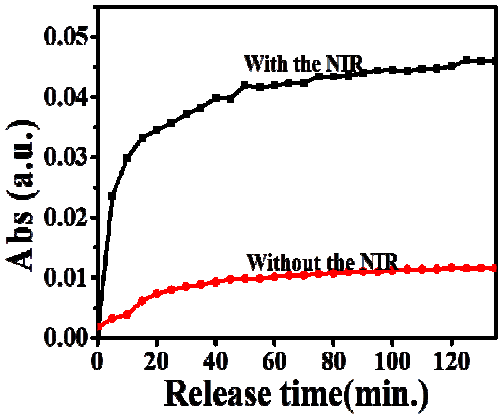

Figure 6. Release profile of MB from the $(rGO/AuNS)_5$ film with and without NIR irradiation, showing that only with irradiation that the MB was effectively released from the multilayered films. The absorbance intensity at 664 nm was used in the plotting.

suggests that the films could be used as drug reservoir and function in an induced-release manner, and thus present low toxicity to the unintended area of the body if used in vivo.

Conclusion

In this report we studied the photothermal effect of the hybrid $(rGO/AuNS)_n$ film, and discussed the pros and cons of the hybrid films in comparison with the single- (photothermal effective) component film of $(PAA/PAH\text{-}rGO)_n$ and $(PAH/AuNS)_n$. For all three types of films, the photothermal effect increased with growing number of assembly. The hybrid films presented the highest photothermal effect compared with $(PAA/PAH\text{-}rGO)_n$ and $(PAH/AuNS)_n$ films with identical cycles of assembly. However, because of the instability of AuNS with irradiation, the photothermal effect of hybrid $(rGO/AuNS)_n$ films deteriorated over time, and about 15% deterioration was observed over 10 cycles of repeated heating and cooling with the heating duration being 5 min for each cycle, but the ultimate heating effect was still higher than the $(PAA/PAH\text{-}rGO)_n$ and $(PAH/AuNS)_n$ films. The hybrid $(rGO/AuNS)_5$ films released model drug MB in a controlled manner adjusted by IR irradiation. With IR irradiation, 78% of the maximum released amount of MB was effectively released within 20 min. However, without irradiation, only 22% of MB was released compared with irradiation. The report demonstrated that the hybrid $(rGO/AuNS)_n$ film serve as effective heating film with drug loading and controlled release properties. We expect this report promote rational design and selection of graphene or AuNS- based photothermal materials in smart devices or medical therapy materials.

Acknowledgements

This work was supported by the NSFC (21303169, 51273030), the Fundamental Research Funds for the Central Universities (2652013115, DUT14ZD217), Beijing Nova Program (Z141103001814064), Beijing Specific Project to Foster Elitist (2013D009015000001), and National High Technology Research and Development Program of China (863 Program 2012AA06A109) and the special co-construction project of Beijing city education committee.

Notes and references

Supporting Information. SEM, AFM images and UV-vis spectra of AuNS, and UV-vis spectra of rGO. This material is available free of charge via the Internet at http://pubs.rsc.org.

1 V. Shanmugam, S. Selvakumar and C. S. Yeh, *Chem. Soc. Rev.,* 2014, **43**, 6254.
2 S. Sortino, *J. Mater. Chem.,* 2012, **22**, 301.
3 C. A. Tao, X. Zou, Z. Hu, H. Liu and J. Wang, Polym. Compos., 2014, **19**,DOI:10.1002/pc.23303.

4 Y. W. Chen, P. J. Chen, S. H. Hu, I. W. Chen and S. Y. Chen, *Adv. Funct. Mater.,* 2014, **24**, 451.
5 A. Bansal and Y. Zhang, *Accounts Chem. Res.,* 2014, **47**, 3052.
6 J. J. Qiu and W. D. Wei, *J. Phys. Chem. C,* 2014, **118**, 20735-20749.
7 X. F. Li, C. Y. Chen, Y. H. Zhao and X. Y. Yuan, *Prog. Biochem. Biophys.* 2014, **41**, 739.
8 W. Xie and S. Schlucker, Rep. Prog. Phys., 2014, 77,116502.
9 H. Kim, D. Lee, J. Kim, T. I. Kim and W. J. Kim, *ACS Nano* 2013, **7**, 6735.
10 C. A. Tao, J. F. Wang, S. Q. Qin, Y. A. Lv, Y. Long, H. Zhu and Z. H. Jiang, *J. Mater. Chem.,* 2012, **22**, 24856.
11 S. X. Shi, F. Chen, E. B. Ehlerding and W. B. Cai, *Bioconjugate Chem.,* 2014, **25**, 1609.
12 R. K. Shervedani and A. Amini, *Electrochim. Acta.,* 2014, **121**, 376.
13 S. Z. Nergiz, N. Gandra, S. Tadepalli, and S. Singamaneni, *ACS Appl. Mater. Interfaces,* 2014, **6**, 16395.
14 X. Bian, Z. L. Song, Y. Qian, W. Gao, Z. Q. Cheng, L. Chen, H.Liang, D. Ding, X. K. Nie, Z. Chen and W. H. Tan, *Sci. Rep.,* 2014, **4**, 6093.
15 D. H. Lin, T. Q. Qin, Y. Q. Wang, X. Y. Sun, and L. X. Chen, *ACS Appl. Mater. Interfaces,* 2014, **6**, 1320.
16 A. F. Zedan, S. Moussa, J. Terner and G. Atkinson, *Acs Nano,* 2013, **7**, 627.
17 D. K. Lim, A. Barhoumi, R. G. Wylie, G. Reznor, R. S. Langer and D. S. Kohane, *Nano Lett.,* 2013, **13**, 4075.
18 Y. Wang, R. Yuan, Y. Q. Chai, Y. L. Yuan and L. J. Bai, *Biosens. Bioelectron.* 2012, **38**, 50.
19 Y. Choi, M. Gu, J. Park, H. K. Song and B. S. Kim, *Adv. Energy Mater.* 2012, **2**, 1510.
20 T. R. Kuo, D. Y. Wang, Y. C. Chiu, Y. C. Yeh, W. T.Chen, C. H. Chen, C. W. Chen, H. C. Chang, C. C. Hu and C. C. Chen, *Anal. Chim. Acta.,* 2014, **809**, 97.
21 Y. Li, X. Wang and J. Q. Sun, *Chem. Soc. Rev.* 2012, **41**, 5998.
22 M. J. Cheng, F. Shi, J. S. Li, Z. F. Lin, C. Jiang, M. Xiao, L. Q. Zhang, W. T. Yang and T. S. Nishi, *Adv. Mater.* 2014, **26**, 3009.
23 J. S. Park, S. M. Cho, W. J. Kim, J. Park, and P. J. Yoo, *ACS Appl. Mater. Interfaces,* 2011, **3**, 360.
24 Y. Zhou, M .J. Cheng, X. Q. Zhu, Y. J. Zhang, Q. An and F. Shi, *ACS Appl. Mater. Interfaces,* 2013, **5**, 8308.
25 K. Ariga, J. P. Hill and Q. M. Ji, *Phys. Chem. Chem. Phys.,* 2007, **9**, 2319.
26 Q. An, Y. Zhou, Y. J. Zhang, Y. H. Zhang and F. Shi, *RSC Adv.,* 2014, **4**, 5683.
27 M. J. Cheng, Q. Liu, Y. M. Xian and F. Shi, *ACS Appl. Mater. Interfaces,* 2014, **6**, 7572.
28 K. Ariga, M. McShane, Y. M. Lvov, Q. M. Ji, J. P. Hill, *Drug Del.,* 2011, **8**, 633.
29 X. K. Liu, H. L. Xu, H. B. Xia and D. Y. Wang, *Langmuir,* 2012, **28**, 13720.
30 P. Jiang, J. J. Zhou, R. Li, Y. Gao, T. L. Sun, X. W. Zhao, Y. J. Xiang and S. S. Xie, *J. Nanopart. Res.,* 2006**, 8**, 927.
31 T. Tang and I. W. Hamley, *Colloid Surface A: Physicochem. Eng. Aspects,* 2009, **336**, 1.
32 K. Chan, L. E. Kostun, W. E. Tenhaeff, K. K. Gleason, *Polymer*, 2006, **47**, 6941.
33 A. J. Mieszawska, W. J. M. Mulder, Z. A. Fayad, D. P. Cormode, *Mol. Pharmaceut.,* 2013, **10**, 831.
34 K. Park, H. Koerner, R. A. Vaia, *Nano lett.,* 2010, **10**, 1433.
35 V. Zucolotto, M. Ferreira, M. R. Cordeiro, C. J. L. Constantino, D. T. Balogh, A. R. Zanatta, W. C. Moreira and O. N. Oliveira, *J Phys Chem B*,2003, **107**, 3733.
36 C. Bonazzola and E. J. Calvo, *Langmuir*, 2003, **19**, 5279.
37 S. A. Sukhishvili and S. Granick, *Macromolecules*, 2002, **35**, 301.

TOC

The photothermal effects of layer-by-layer AuNS (gold nanosheets)/rGO hybrid films outperformed that of rGO or AuNSs films under NIR irradiation.